Piezoelectric networking with enhanced electromechanical coupling for vibration delocalization of mistuned periodic structures—Theory and experiment

Hongbiao Yu[a], K.W. Wang[b],*, Jianhua Zhang[c]

[a]*The Pennsylvania State University, 7 Hammond Building, University Park, PA 16802, USA*
[b]*The Pennsylvania State University, 157 Hammond Building, University Park, PA 16802, USA*
[c]*The Pennsylvania State University, 229 Hammond Building, University Park, PA 16802, USA*

Abstract

In this research, an approach to vibration delocalization of nearly periodic structures using piezoelectric networks with active coupling enhancement is presented. Piezoelectric networks are synthesized to reduce mode localization by absorbing the vibratory mechanical energy into the electric circuits and distributing it through an additional strong electrical wave channel. The system electromechanical coupling effect is further increased through the use of active actions via negative capacitance circuits, which will enhance the treatment's delocalization capability. The integrated system is analyzed through modal analysis and transfer matrix analysis. A localization index is defined based on the Lyapunov exponent and used to evaluate the effectiveness of the proposed treatment. Experiments are carried out to validate the theoretical findings. The results demonstrated that, for the range of investigation, the system vibration localization level can be effectively reduced by piezoelectric networking, and the system performance can be further improved by the active coupling enhancement approach via negative capacitance circuits.

© 2006 Elsevier Ltd. All rights reserved.

1. Introduction

Periodic structures have been widely applied in a variety of engineering applications, such as turbomachinery bladed-disks, satellite antennae and space trusses. These structures are designed to contain identical substructures that form a spatial periodicity. In an ideal situation, where the substructures are indeed identical, the vibration energy is uniformly distributed over the substructures, and mode shapes are extended throughout the substructures without attenuation. However, in realistic situations, there are always small differences among the substructures, hereafter referred to as *mistuning*, such as blade-to-blade differences in geometry and material properties due to variation in material properties, manufacturing tolerance, and in-service degradation, etc. These small mistuning could change the dynamic behavior of the periodic structures (now become so-called *nearly* or *mistuned* periodic structures) drastically compared to that of the perfect

*Corresponding author. Tel.: +1 814 865 2183; fax: +1 814 863 7222.

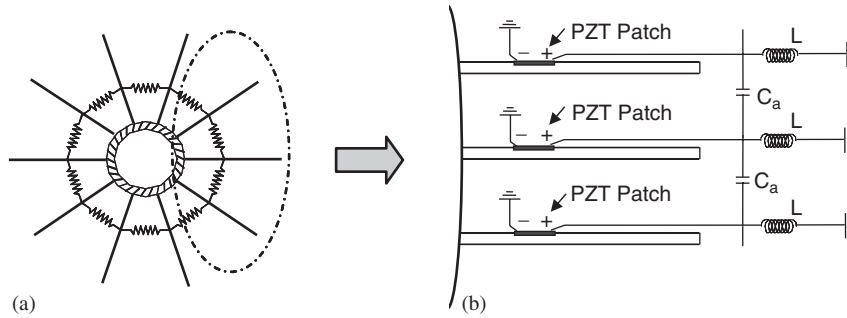*E-mail address:* kwwang@psu.edu (K.W. Wang).

Fig. 1. (a) Schematic of period structure and (b) periodic structure integrated with coupled piezoelectric circuit network.

structures. A phenomenon known as *localization* could occur under certain circumstances [1–4], especially when the couplings among substructures are weak. In a localized mode, vibration energy is confined to a small region of the structure, resulting in increased stresses and amplitudes locally. The occurrence of mode localization could cause severe damage to the structure.

To date, most of the relevant research has concentrated on exploring the cause of vibration localization [5–8] and predicting the localized response [9–13]. The dynamic properties of periodic structures have often been studied from a wave perspective [14,15] utilizing the transfer matrix approach and the Lyapunov exponents were frequently used to characterize localization [16–19]. While research on these fundamental aspects of localization is extensive, few studies have been performed in developing methods to reduce or control vibration localization in nearly periodic structures. Castanier and Pierre [20] explored the feasibility of using intentional mistuning to decrease the localization effects in turbo-machinery rotors. Following the principle that higher coupling among substructures will reduce localization, Gordon and Hollkamp [21] investigated the potential of utilizing piezoelectric strain actuators to increase blade-to-blade coupling of bladed disks, and found that the improvement was marginal. Cox and Agnes [22] attempted to reduce vibration localization in bladed-disk assemblies by using embedded piezoelectric patches to increase mechanical coupling ratio between blades. It was found that directly shorting the piezoelectric patches had little effect on reducing localization [22]. An inductive element [23] was later added to the shorted piezoelectric patches, where it was observed that this addition could enhance the system coupling, however, the illustrative example only showed improvement in some of the localized modes. Recently, Tang and Wang [24] proposed a new approach for vibration delocalization via piezoelectric circuitry networking. An example of networking configuration is shown in Fig. 1. In this case, the original mono-coupled system becomes a bi-coupled system with an additional electrical coupling. In general, an inductive piezoelectric circuit (LC shunt) can absorb vibration energy from the substructure to which it is attached and store that portion of energy in the electrical form. While in most cases directly increasing the mechanical coupling between substructures is difficult to achieve due to various design limitations, one can easily introduce strong electrical coupling, such as connecting the LC shunts with capacitors as shown in Fig. 1(b), to create a new wave channel. With this coupled piezoelectric circuits design, the otherwise localized vibration energy in a nearly periodic structure can now be transferred into electrical form and propagate in the integrated system through the newly created electromechanical wave channel. Zhang and Wang [25] have further found that vibration dissipation and suppression can be achieved by including resistive elements in such circuits. For a mistuned periodic structure under forced excitation, it was shown that the treatment can suppress vibration effectively and also create a more uniform distribution of response amplitudes among substructures.

2. Problem statement, research objective and approach overview

While the recent investigations [24,25] have illustrated promising delocalization results utilizing piezoelectric networks, the studies are still preliminary. The concept has not been thoroughly examined via a

comprehensive parameter study, and it has not been realized and validated through actual circuitry design. Most of all, it was recognized that the effectiveness of the treatment can be limited by the level of electromechanical coupling of the piezoelectric patches. From observing Fig. 1, one can see that since the electrical coupling established through the external capacitors can be easily adjusted, the performance bottleneck of the piezoelectric network is the electromechanical coupling, i.e., how much mechanical energy can be transferred into electrical energy. For most of the cases investigated in previous studies, the electromechanical coupling coefficient is not high enough to ensure that all the modes be significantly delocalized. In other words, while the degrees of localization of all the modes were reduced with the treatment, the improvements in some modes were marginal. This coupling coefficient is determined by the piezoelectric material property, the size and the location of patches on the host structures, and the stiffness of the host structures. Thus it is in general difficult to change with only passive designs.

Based on the above observations, the objectives of this research are: (1) to explore the possibility of utilizing an active coupling enhancement approach to increase the system electromechanical coupling, such that the effectiveness of the piezoelectric network for delocalization can be better improved; (2) to analyze the integrated system and quantitatively evaluate the delocalization effect; and (3) to implement and validate the proposed concept experimentally. In this study, the negative capacitance circuit approach [26] is proposed and investigated for active coupling enhancement. In this paper, the possibility of increasing the system generalized electromechanical coupling coefficient by using negative capacitance is discussed and the relationship between the negative capacitance and the coupling coefficient is presented. An integrated system consisting of a mistuned periodic structure with the piezoelectric network is modeled, and based on this model, the mode shapes of the mistuned system are investigated and the Lyapunov exponents are derived. The correlation between the Lyapunov exponents and the spatial exponential decay of the modal amplitudes is discussed. A localization index is then defined and used to evaluate the effect of the negative capacitance on the system's delocalization performance. Finally, a series of experiments are carried out to validate the aforementioned delocalization ideas.

3. System model

To maintain simplicity, the periodic structure considered in this research is assumed to consist of N identical cantilever beams coupled by N springs, as shown in Fig. 1(a). Lumped springs are used to emulate the coupling effects in generic periodic structures. The network topology, integrated with the host periodic structure, is shown in Fig. 1(b).

In this configuration, an inductive piezoelectric shunt circuit (piezoelectric patch connected in series with an inductor) is applied to each of the substructures in order to absorb the vibration energy and transform it into electric form. Then these individual local circuits are coupled through capacitive elements to form a global network. This network topology creates an additional wave channel, through which the localized vibration energy can be propagated.

Let ϕ be the first local beam mode without the piezoelectric shunt circuits. The transversal displacement of the jth beam is approximated as

$$w_j(x,t) \approx \phi(x)q_j(t). \tag{1}$$

The equations of motion for the periodic structure integrated with piezoelectric patches can be derived using Hamilton's principle [24], which are

$$m\ddot{q}_j + g\dot{q}_j + kq_j + k_1 Q_j + k_c(q_j - q_{j-1}) + k_c(q_j - q_{j+1}) = f_j, \tag{2}$$

$$k_2 Q_j + k_1 q_j = V_j, \tag{3}$$

where m, g, k, k_c, k_1 and k_2 are, respectively, mass, damping, substructure stiffness, substructure coupling stiffness, cross coupling coefficient related to the electromechanical coupling of the piezoelectric patch, and

inverse of the capacitance of the piezoelectric patch, given by

$$m = \int_0^{l_b} \rho_b A_b \phi^2 \, \mathrm{d}x + \int_0^{l_b} \rho_p A_p \phi^2 \, \Delta H \, \mathrm{d}x, \quad g = \int_0^{l_b} g_b \phi^2 \, \mathrm{d}x,$$

$$k = \int_0^{l_b} E_b I_b \phi''^2 \, \mathrm{d}x + \int_0^{l_b} E_p I_p \phi''^2 \, \Delta H \, \mathrm{d}x, \quad k_c = k_s \phi^2(x_s),$$

$$k_1 = \frac{1}{w_p l_p} \int_0^{l_b} F_p h_{31} \phi'' \Delta H \, \mathrm{d}x, \quad k_2 = \frac{A_p \beta_{33}}{w_p^2 l_p}.$$

Here, q_j and f_j are the generalized mechanical displacement and external force of the jth beam. Q_j and V_j are the charge flowing to and the voltage across the piezoelectric patch attached to the jth beam, respectively. $\Delta H = H(x - x_l) - H(x - x_r)$, where $H(x)$ is the Heaviside step function. x_l and x_r are distances from the piezoelectric patch edges to the root of the cantilever beam, and the length of the patch is thus $l_p = x_r - x_l$. Other relevant notations used here are: ρ_b and ρ_p the density of beam and piezoelectric patch; A_b and A_p the cross section area of beam and piezoelectric patch; E_b and E_p the elastic modulus of beam and piezoelectric patch; I_b and I_p the moment of inertial of beam and piezoelectric patch; l_b the length of beam; w_p the width of piezoelectric patch; F_p the moment of area of piezoelectric patch; g_b the beam damping constant; k_s and x_s the stiffness of coupling spring and location of coupling spring; h_{31} the piezoelectric constant; and β_{33} the dielectric constant of piezoelectric patch.

Applying circuit network analysis to Fig. 1(b), the equation for the jth circuit branch can be derived as

$$V_j = -L\ddot{Q}_j - \frac{L}{k_a} k_2 (2\ddot{Q}_j - \ddot{Q}_{j-1} - \ddot{Q}_{j+1}) - \frac{L}{k_a} k_1 (2\ddot{q}_j - \ddot{q}_{j-1} - \ddot{q}_{j+1}), \tag{4}$$

where L is the circuitry inductance. $k_a = 1/C_a$ denotes the inverse of the coupling capacitance. Substituting Eq. (4) into Eq. (3), we can derive the equations of motion of the electromechanically integrated system as

$$m\ddot{q}_j + g\dot{q}_j + kq_j + k_1 Q_j + k_c(q_j - q_{j-1}) + k_c(q_j - q_{j+1}) = f_j, \tag{5}$$

$$L\ddot{Q}_j + \frac{L}{k_a} k_2 (2\ddot{Q}_j - \ddot{Q}_{j-1} - \ddot{Q}_{j+1}) + \frac{L}{k_a} k_1 (2\ddot{q}_j - \ddot{q}_{j-1} - \ddot{q}_{j+1}) + k_2 Q_j + k_1 q_j = 0. \tag{6}$$

For the original periodic structure without the piezoelectric circuits, the equation of motion is

$$m\ddot{q}_j + g\dot{q}_j + kq_j + k_c(q_j - q_{j-1}) + k_c(q_j - q_{j+1}) = f_j. \tag{7}$$

In the above derivation, we assume that the system is perfectly periodic. In reality, however, there will be imperfections. Without loss of generality, in this paper we assume that the structural imperfection (mistuning) exists in the substructural mechanical stiffness, which is the common practice in many localization studies. The stiffness of the jth beam with mistuning is

$$\tilde{k}_j = k + \Delta k_j, \tag{8}$$

where k is the nominal stiffness of the perfectly periodic structure, and Δk_j is the zero-mean random mistuning in stiffness. In the following, we consider harmonic solutions for free vibration, and neglect damping, the non-dimensionalized equations of motion of the electromechanically integrated system become

$$-\Omega^2 x_j + (1 + \Delta s_j)x_j + R_c^2(x_j - x_{j-1}) + R_c^2(x_j - x_{j+1}) + \delta\xi y_j = 0, \tag{9a}$$

$$-\Omega^2 \left[y_j + R_a^2(2y_j - y_{j-1} - y_{j+1}) + \frac{\xi R_a^2}{\delta}(2x_j - x_{j-1} - x_{j+1}) \right] + \delta\xi x_j + \delta^2 y_j = 0 \tag{9b}$$

and the equation for the mistuned system without piezoelectric network becomes

$$-\Omega^2 x_j + (1 + \Delta s_j)x_j + R_c^2(x_j - x_{j-1}) + R_c^2(x_j - x_{j+1}) = 0, \tag{10}$$

where

$$\omega_m = \sqrt{k/m}, \quad \omega_e = \sqrt{k_2/L}, \quad \delta = \omega_e/\omega_m,$$

$$\Omega = \omega/\omega_m, \quad x_j = \sqrt{m}q_j, \quad y_j = \sqrt{L}Q_j,$$

$$\xi = k_1/\sqrt{kk_2}, \quad R_c = \sqrt{k_c/k}, \quad R_a = \sqrt{k_2/k_a}, \quad \Delta s_j = \Delta k_j/k.$$

Here ω and Ω are the dimensional and non-dimensional harmonic frequencies; ω_m and ω_e are the natural frequencies of the uncoupled substructure and circuit, respectively; δ is the frequency tuning ratio which characterizes the circuitry inductance; x_j and y_j are the generalized mechanical and electrical displacements of the jth substructure and circuit branch respectively; ξ is the generalized electromechanical coupling coefficient which reflects the energy transfer capability of the piezoelectric patch; R_c is the mechanical coupling ratio between the substructures; R_a is the electrical coupling ratio related to the coupling capacitance; and Δs_j is the mistuning ratio which is a zero-mean random number with standard deviation σ_m.

4. Active coupling enhancement

The generalized electromechanical coupling coefficient (ξ) plays an important role in the piezoelectric network delocalization mechanisms, since it characterizes the amount of energy that can be transformed from mechanical into electrical form. Although previous studies have shown promising delocalization results using the proposed piezoelectric network, it was also recognized that the improvements in some modes were marginal due to the low electromechanical coupling coefficient ξ. It should be noted that this generalized electromechanical coupling coefficient is not the same as the intrinsic coupling factor of the material itself. For piezoelectric materials, the electromechanical coupling factor is a non-dimensional number quantifying the energy conversion capability of the materials, the definition of which can be found in Ref. [27]. The definition of the coupling factor (k_m) is based on the material stiffness at open circuit (constant electric displacement) condition (c^D) and at short circuit (constant electric field) condition (c^E), and can be expressed as [28]: $k_m^2 = (c^D - c^E)/c^D$. The material coupling factor has different values corresponding to different conditions. For the patch application considered in this study (i.e., in the 3–1 direction application where the uniaxial stress is perpendicular to the poling direction), the coupling factor is about 0.35. The largest coupling factor for polycrystalline piezoelectric ceramic materials can be on the order of 0.7, corresponding to an energy conversion factor of about 50% [28]. When devices made of piezoelectric materials are integrated in a structure, the generalized electromechanical coupling coefficient ξ can be defined at the structural level [28]. The coupling coefficient can be calculated based on the structural open circuit natural frequency (ω^D) and short circuit natural frequency (ω^E): $\xi = \sqrt{(\omega^D)^2 - (\omega^E)^2}/\omega^D$. This value is in general smaller than the intrinsic electromechanical coupling factor of the material itself. The formula of the generalized electromechanical coupling coefficient, $\xi = k_1/\sqrt{kk_2}$ used in this study, is consistent with the above definition, which can be easily derived and verified from Eqs. (2) and (3) when the open and short circuit conditions are applied [26]. It is clear that in a dynamical system, this generalized electromechanical coupling coefficient is a function of the cross coupling term k_1, the stiffness of the host structure k, and the inverse of the piezoelectric capacitance k_2. To obtain a higher ξ, one can either increase k_1, or decrease k and k_2. Since k_1 is usually fixed once the material type (thus the material coupling factor), the size and the location of the piezoelectric patch on the host structure is determined, it is difficult to be increased due to practical limitations. On the other hand, to increase the generalized electromechanical coupling coefficient, one can also tune k and k_2. Lesieutre and Davis [28] proposed a method using destabilizing mechanical pre-loads to counter the inherent stiffness, thus to reduce the stiffness k of the host structure, and increase the apparent coupling coefficient. Although this method is indeed interesting, it might be difficult to implement since it usually requires pre-conditioning or modification of the host structure. Recently, Tang and Wang [26] proposed a negative capacitance circuit approach to partially cancel the inherent capacitance of the piezoelectric patch, which will reduce the electrical stiffness k_2 and increase the coupling coefficient ξ. Such an approach can be easily realized utilizing an electric circuit, which is much easier to implement than changing k and k_1 via mechanical tailoring. In this study, this negative capacitance approach is adopted to increase the generalized electromechanical coupling coefficient, for the purpose of enhancing the delocalization performance of the network.

In the formula $\xi = k_1/\sqrt{kk_2}$, k_2 is the inverse of the piezoelectric capacitance. When a negative capacitance is added in series to the piezoelectric element in the network, the inverse of the total capacitance in each branch of the piezoelectric network becomes

$$\hat{k}_2 = k_2 - k_n, \tag{11}$$

where k_n is the inverse of the negative capacitance added. With the negative capacitance, the generalized electromechanical coupling coefficient becomes

$$\xi = k_1/\sqrt{k\hat{k}_2}. \tag{12}$$

Since $\hat{k}_2$ is less than k_2 (Eq. (11)), it is obvious that the generalized electromechanical coupling coefficient (ξ) can be increased by the negative capacitance treatment. However, to ensure stability of the system, there is a limit on the negative capacitance, which is governed by maintaining the positive definiteness of the system generalized stiffness matrix

$$\begin{bmatrix} k & k_1 \\ k_1 & \hat{k}_2 \end{bmatrix} > 0, \tag{13}$$

which means $k\hat{k}_2 > k_1^2$ or $\xi < 1$.

From Eq. (11), it is clear that k_n must be less than k_2, or in other words, the absolute value of the negative capacitance should be larger than the piezoelectric capacitance. The relationship between the generalized electromechanical coupling coefficient and the negative capacitance is given in Fig. 2, where the coupling coefficient for the original system without negative capacitance is assumed to be 0.1, and the ratio of k_n/k_2 is referred to as the *negative capacitance ratio*. It can be seen that the coupling coefficient can increase monotonically and nonlinearly as the negative capacitance ratio (k_n/k_2) increases. The closer the negative capacitance value is to the piezoelectric capacitance, i.e., the closer the negative capacitance ratio (k_n/k_2) is to 1, the larger the coupling coefficient would be. However, in practice, the circuit will be vulnerable to instability as the ratio gets closer to 1, as indicated by Eq. (13). The negative capacitance cannot be realized passively and one needs to use an operational amplifier to form a negative impedance converter circuit that requires a power source. Therefore, this approach is referred to as an active coupling enhancement approach.
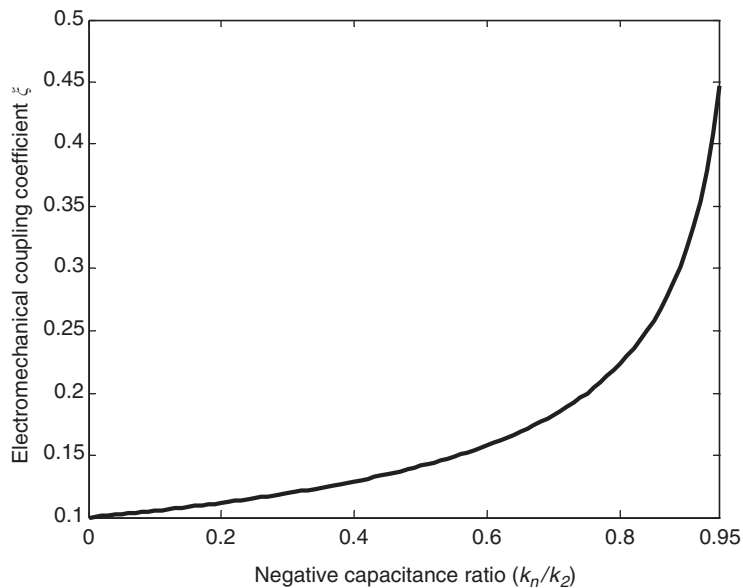

Fig. 2. Effect of negative capacitance on the electromechanical coupling coefficient.

5. Integrated system analysis

As indicated earlier, the localization phenomenon in mistuned periodic structures has been analyzed extensively in the past. The probabilistic nature of the localization phenomenon was recognized and stochastic methods were applied to study the spatial exponential decay rate of the vibration amplitude [3,9,16]. Lyapunov exponents of the global stochastic wave transfer matrix have been introduced to approximate the spatial exponential decay rate of the amplitude, and have been shown to be a good measure of the localization level [3,16–19]. The wave transfer matrix method and the numerical computation of the Lyapunov exponents for multi-coupled periodic structures have been discussed by Pierre et al. [3]. To formulate the wave transfer matrix expression for the bi-coupled system presented in this paper, a displacement state vector is defined for each bay (a bay consists of two adjacent substructures). Then the transfer matrix that relates the dynamics of two adjacent bays can be derived from the equations of motion. The dimension of the state vector is always twice the number of inter-bay coupling coordinates m, and the dimension of the square transfer matrix is $2m \times 2m$, which is independent of the number of substructures N. The wave transfer matrix for the original system without piezoelectric network can be found in Ref. [24]. Below, only the formulation for the system with integrated piezoelectric network is presented. This integrated system is bi-coupled, thus the inter-bay coupling is $m = 2$, and the dimensions of the displacement state vector and transfer matrix are 4×1 and 4×4, respectively. The 4×1 displacement state vector for the jth bay, consisting of both mechanical and electrical generalized displacements from the jth and the $j+1$th substructures, is defined as

$$\mathbf{u}_j = [x_{j+1}\ y_{j+1}\ x_j\ y_j]^{\mathrm{T}}. \tag{14}$$

The system equations Eqs. 9(a) and (b) can be rewritten into the transfer matrix expression using the displacement state vector:

$$\mathbf{u}_j = \mathbf{T}_j \mathbf{u}_{j-1}, \tag{15}$$

where $\mathbf{T}_j$ is the 4×4 transfer matrix given by Eq. (16):

$$\mathbf{T}_j = \begin{bmatrix} \frac{1+2R_c^2+\Delta s_j-\Omega^2}{R_c^2} & \frac{\delta\xi}{R_c^2} & -1 & 0 \\ -\left(\frac{\delta\xi}{\Omega^2 R_a^2} + \frac{\xi}{\delta}\left(\frac{1+\Delta s_j-\Omega^2}{R_c^2}\right)\right) & -\left(\frac{\delta^2}{\Omega^2 R_a^2} - (2+1/R_a^2) + \frac{\xi^2}{R_c^2}\right) & 0 & -1 \\ 1 & 0 & 0 & 0 \\ 0 & 1 & 0 & 0 \end{bmatrix}. \tag{16}$$

Obviously, the transfer matrix is random for mistuned structures because of the random mistuning Δs_j. For tuned structures, $\Delta s_j = 0$, and $\mathbf{T}_j$ is identical for all j's. A Lyapunov exponent is defined as

$$\gamma(\mathbf{u}_0) = \lim_{N\to\infty}\frac{1}{N}\log\|\mathbf{u}_N\|, \tag{17}$$

where $\mathbf{u}_0$ is the initial displacement state vector and $\mathbf{u}_N$ is the displacement state vector of the Nth substructure. It can be shown that the Lyapunov exponent can be calculated from the product of the transfer matrices [24]:

$$\gamma_k = \lim_{N\to\infty}\frac{1}{N}\log\left\{\sigma_k\left(\prod_{j=N}^{1}\mathbf{T}_j\right)\right\}, \tag{18}$$

where $\sigma_k(\cdot)$ denotes the singular value operator.

In this study, the Lyapunov exponents of the bi-coupled periodic structure integrated with piezoelectric network are calculated using Wolf's algorithm [29]. The number of Lyapunov exponents equals to twice the number of coupling coordinates. For this bi-coupled system, there are four Lyapunov exponents in total. In fact, these Lyapunov exponents appear in pairs, with same magnitude but opposite signs, $\pm|\gamma|$. For a periodic structure, both these positive and negative Lyapunov exponents share the same physical meaning. Therefore, calculating the positive Lyapunov exponents is sufficient to identify the entire spectrum. In the following discussion, *Lyapunov exponents* by default refer to the positive ones unless otherwise noted.

For this study, the structural damping and circuitry resistance are neglected so that the vibration localization effect can be clearly identified. The original periodic structure without piezoelectric network is a mono-coupled system, so there is only one Lyapunov exponent and mode localization can be directly evaluated by the Lyapunov exponent, as demonstrated in Refs. [3,24]. For the periodic structure with the piezoelectric network treatment, the introduction of the strong electrical coupling enabled by the capacitors between the local shunt circuits creates another wave channel. Therefore, the system becomes bi-coupled; and there are two Lyapunov exponents at each frequency. Fig. 3 shows the Lyapunov exponents for the system with parameters $\xi = 0.1$, $R_a = 0.6$, $\delta = 1.2$, $R_c = 0.005$, and $\sigma_m = 0.01$. Here Fig. 3(a) is for the tuned case, Fig. 3(b) is for the mistuned case and Fig. 3(c) provides a zoom-in view around $\Omega = 1$ for both the tuned and mistuned cases. The two Lyapunov exponents are referred to as upper and lower branches in Fig. 3. For this system, as indicated in Fig. 3(a), there are two separate passbands (referred to as passband 1 and passband 2) for the tuned case. The natural frequencies are found to be inside the passbands. It is well known that mode shapes of the tuned system are extended without attenuation throughout the substructures, or in other words, having zero decay rates. This characteristic of tuned system is captured by the zero Lyapunov exponents in the passbands. When the system has mistuning, there are no longer any passbands; and the lower Lyapunov exponent branch becomes non-zero (see the lower dotted line in Fig. 3(c)), indicating mode localization caused by mistuning. When localization occurs, the localized modal amplitudes will have a spatial exponential decay,
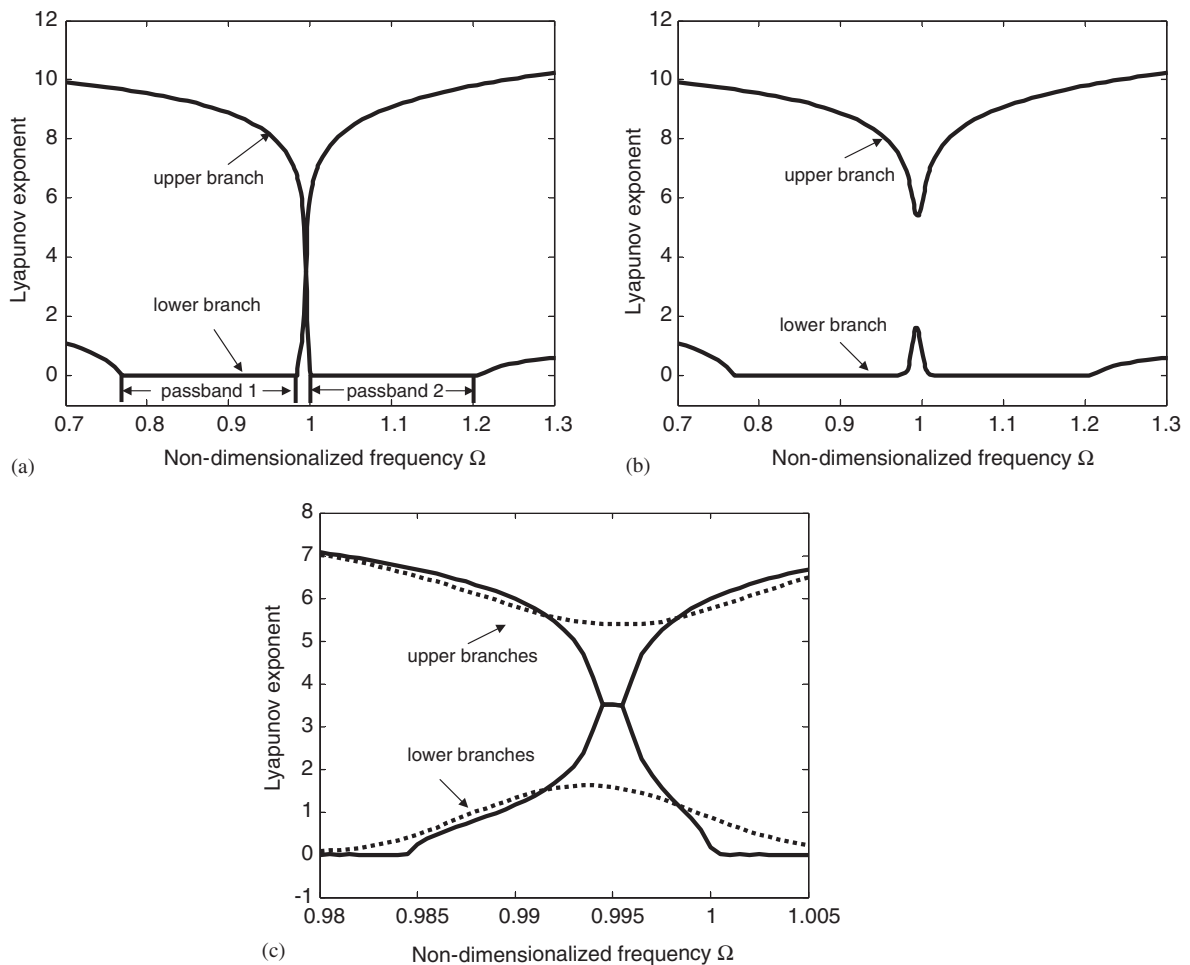

Fig. 3. Lyapunov exponents for the system with piezoelectric network ($\xi = 0.1$, $R_a = 0.6$, $\delta = 1.2$, $R_c = 0.005$, $\sigma_m = 0.01$): (a) tuned system; (b) mistuned system; and (c) zoom-in of tuned (solid lines) and mistuned (dotted lines) system around $\Omega = 1$.

the rate of which can be approximated by the lower one of the two Lyapunov exponents in the original separate passbands.

To support the above argument, the correlation of the modal amplitude exponential decay rates and the lower Lyapunov exponents is studied. In the following analysis, mode shapes of the mistuned periodic structure with piezoelectric network are obtained by solving the eigenvalue problem of the system, the parameters of which are the same as those used for Fig. 3. For modal analysis, the mistuned periodic structure is assumed to have $N = 80$ substructures. To demonstrate the exponential decay of the modal amplitudes, the substructure which has the highest amplitude is chosen as the first substructure. Two examples are demonstrated in Fig. 4. Amplitudes of two modes are shown, the 70th mode with natural frequency of $\Omega = 0.9832$, which lies in the original passband 1 and the 93rd mode with natural frequency of $\Omega = 1.0006$, which lies in the original passband 2. The amplitudes of the 70th mode in logarithm scale are plotted as a dotted line. It is shown that the modal amplitudes decay exponentially throughout the first half of the substructures. Actually, the exponential growth in the second half of the substructures can be seen as exponential decay at the same rate towards the other direction, due to the cyclic nature of the periodic structure. At its natural frequency $\Omega = 0.9832$, the upper and lower Lyapunov exponents are computed to be 6.6969 and 0.2720, respectively. The dash-dotted line is a straight line with a slope of -0.2720, which is directly related to the lower Lyapunov exponent. It can be seen that the exponential decay rate for the 70th mode is well captured by this straight line, which means, the lower Lyapunov exponent can characterize the exponential decay of the modal amplitude. Another example is the 93rd mode, with natural frequency of $\Omega = 1.0006$. At this frequency, the upper and lower Lyapunov exponents are calculated to be 5.8572 and 0.7202, respectively. The modal amplitudes in natural logarithm scale are plotted as a solid line in Fig. 4. The dashed straight line has a slope of -0.7202, corresponding to the lower Lyapunov exponent at this frequency. Obviously, this straight line can approximate the spatial exponential decay of the mode amplitudes very well. Based on the correlation study, we conclude that it is the lower Lyapunov exponent that can characterize the exponential decay of the mode localization for the mistuned system. Therefore, the lower Lyapunov exponent can be served as a measure to quantify the level of the modal localization.

From the above argument, a mode localization index can be defined as the average of the lower Lyapunov exponents of the mistuned system within the frequency range where the original tuned system exhibits two
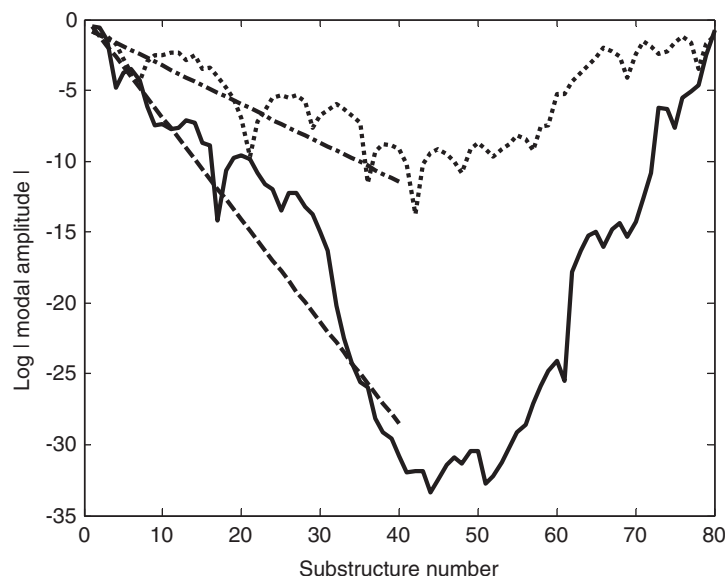

Fig. 4. Correlation of modal amplitudes exponential decay rates to the lower Lyapunov exponents. Solid line: modal amplitude of the 93rd mode ($\Omega = 1.0006$); dashed line: straight line with slope (-0.7202) corresponding to the lower Lyapunov exponent at $\Omega = 1.0006$. Dotted line: modal amplitude of the 70th mode ($\Omega = 0.9832$); dash-dotted line: straight line with slope (-0.2720) corresponding to the lower Lyapunov exponent at $\Omega = 0.9832$.
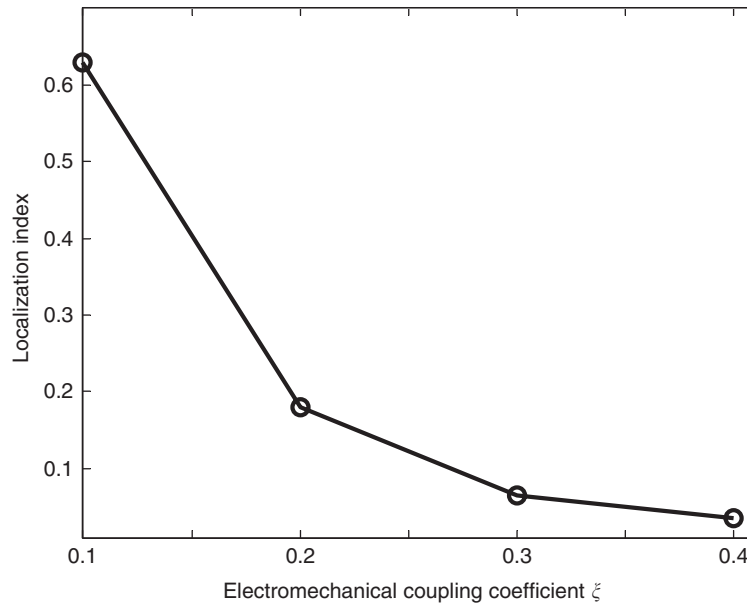
Fig. 5. Localization index versus electromechanical coupling coefficient ξ for the mistuned system ($R_a = 0.5, \delta = 0.5, R_c = 0.005, \sigma_m = 0.01$).

separate passbands. The effect of negative capacitance on mode delocalization performance of the piezoelectric network can now be evaluated using the defined index. In the following parametric study, the average of the lower Lyapunov exponents is taken over 50 frequency points in each passband. As discussed earlier, the introduction of negative capacitance into the piezoelectric network can increase the generalized electromechanical coupling coefficient ξ. To examine the consequence of this coupling enhancement, a single case is first illustrated. In this case study, the system parameters are set to be $R_a = 0.5$, $\delta = 0.5$, $R_c = 0.005$, $\sigma_m = 0.01$. It is shown in Fig. 5 that the localization index decreases as the electromechanical coupling coefficient is increased by adding the negative capacitance. Without negative capacitance ($\xi = 0.1$), the localization index is more than 0.6; with negative capacitance, as the electromechanical coupling coefficient ξ is increased, the localization index can be reduced to as low as values below 0.1. This reduction in localization index indicates that the level of localization is reduced by the introduction of the negative capacitance.

To gain more insight, a more extended parameter study on the effect of negative capacitance on the delocalization performance of the system is carried out using the localization index. The system parameters ξ, R_a and δ are varied within realistic application ranges, which cover the operation parameter region of the experimental study (see next section). Figs. 6 and 7 show the contour plots of the localization index versus ξ and R_a (or δ). In Fig. 6, δ is fixed at 0.5, ξ and R_a are varied. In Fig. 7, R_a is fixed at 1.2, ξ and δ are varied. As shown in both of these two figures, the localization index tends to decrease as ξ increases. These results indicate that as a consequence of increasing the electromechanical coupling coefficient by negative capacitance, the delocalization performance of the piezoelectric network can be improved. Physically, this is because by increasing the system electromechanical coupling coefficient one could increase the capability of energy transformation, thereby more localized mechanical energy can be transferred into electrical form and propagate throughout the network.

6. Experimental investigation

In this investigation, experiments are conducted to validate the concepts of vibration delocalization using the piezoelectric network presented in Fig. 1(b). The effectiveness of negative capacitance on the delocalization performance of the network is also examined.
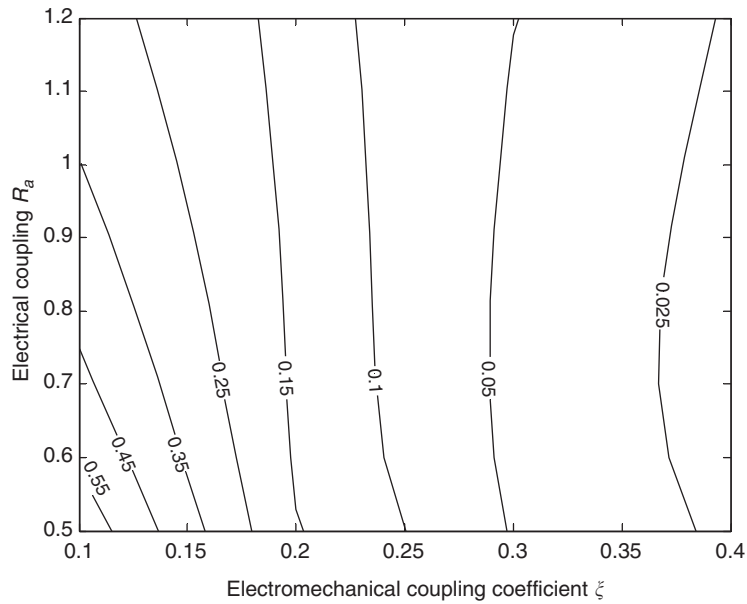
Fig. 6. Contour plot of localization index versus R_a and ξ for the mistuned system ($R_c = 0.005, \delta = 0.5, \sigma_m = 0.01$).
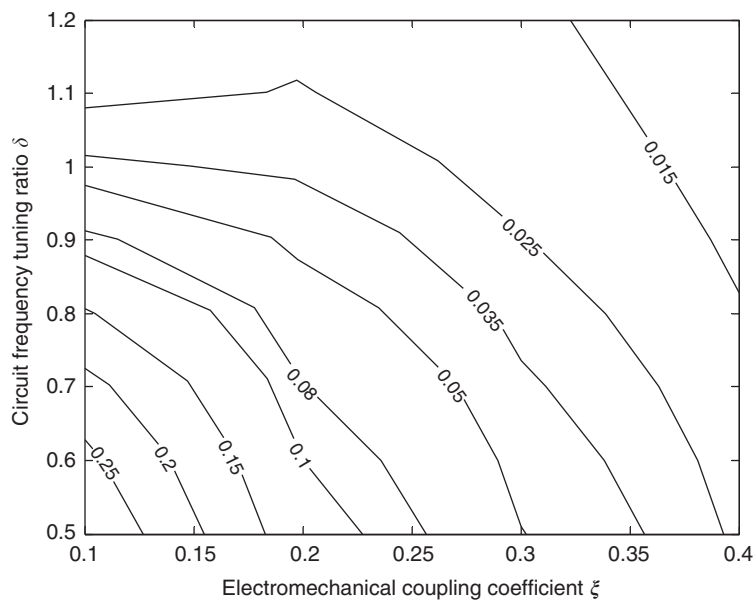

Fig. 7. Contour plot of localization index versus δ and ξ for the mistuned system ($R_c = 0.005, R_a = 1.2, \sigma_m = 0.01$).

6.1. Experimental setup

The overall experimental setup is shown in Fig. 8. The mistuned bladed disk is vertically bolted at the hub disk center to a fixture mounted on an isolation table. A shaker is used to provide excitation at the disk hub. Tip displacements of the blades are measured by a laser vibrometer (OFV-303, Polytec Germany), which converts the displacement information into a voltage related output (calibrated in μm/V or 10^{-6} m/V). This voltage related output is then recorded by an HP35665A analyzer. The resolution of the vibrometer could be as high as 0.5 μm/V. The laser vibrometer is mounted on two perpendicular stages (*X*–*Y* stages as shown in
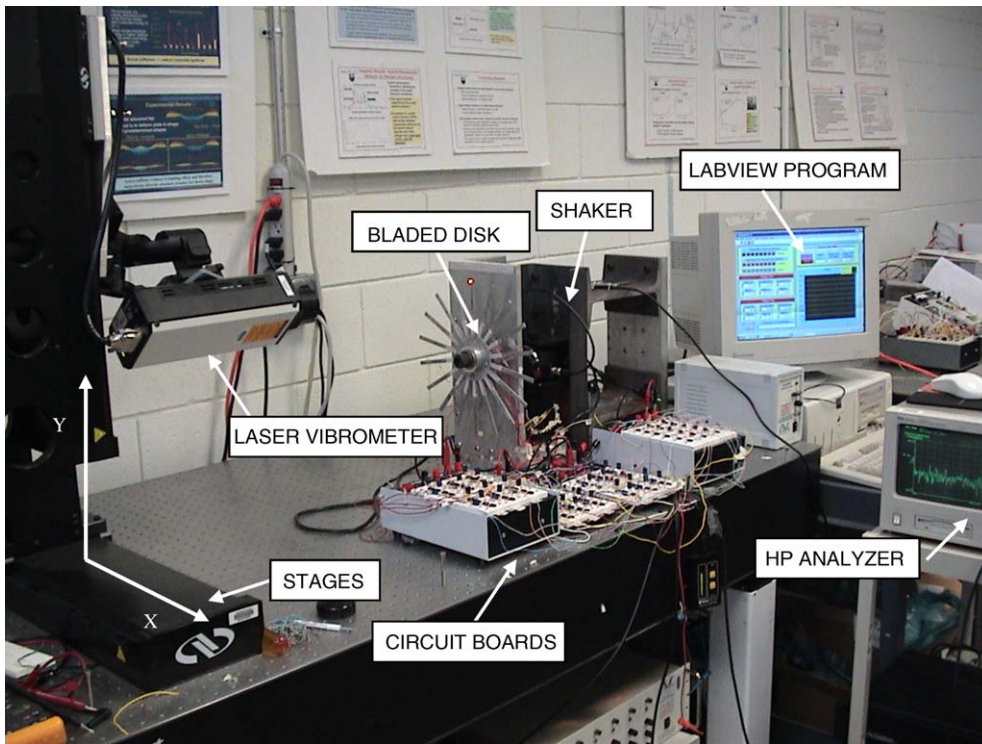
Fig. 8. Overall experimental setup.

Table 1
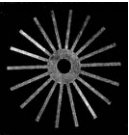Figure and dimensions of the bladed disk model

	Dimensions (10^{-2} m)
	Inner (hole) diameter of the hub disk: 3.81 Outer diameter of the hub disk: 8.89 Length of blade: 10.80 Width of blade: 0.77 Thickness of blade: 0.32

Fig. 8), which, controlled by LabVIEW programs, can precisely locate the measurement point on each blade tip. The bladed disk specimen with 18 equally spaced blades is fabricated from a single piece of aluminum alloy plate (figure and dimension are listed in Table 1), which is mistuned due to manufacturing tolerances. Each blade is bonded with an identical piezoelectric patch (type 5A, APCI, Ltd., properties shown in Table 2) at its root. The bonding process of the piezoelectric patches also contributes to the mistuning of the bladed disk. Therefore, the term *mistuned bladed disk* in the following experimental context refers to the bladed disk with piezoelectric patches attached to it. Each piezoelectric patch has a negative electrode wrap-up design, which improves the bonding effectiveness and provides convenience in wiring. The patches are electrically insulated from the aluminum blades since later on the negative capacitance circuits will be inserted between the piezoelectric patches and the ground. The piezoelectric circuit network is synthesized and integrated with the bladed disk as shown in Fig. 1(b). Each passive piezoelectric patch is connected in series with a synthetic inductor to form an *LC* shunt circuit. Then these 18 shunt circuits are coupled through capacitors (C_a) each with a value of 2.2 nF (corresponding to non-dimensional $R_a = 1.2$, as studied in Fig. 7).

Table 2
Geometric parameters and material properties of piezoelectric patches

Geometry (10^{-2} m)	Material property
Length: 2.54	Piezoelectric material: Type 5A
	Relative dielectric constant K^T: 1750
Width: 0.76	Electromechanical coupling factor k_{31}: 0.36
	Piezoelectric charge constant: 175×10^{-12} (m/V)
Thickness: 0.10	Young's modulus: 6.3×10^{10} (N/m^2)
	Capacitance (C_p): 3.3 nF
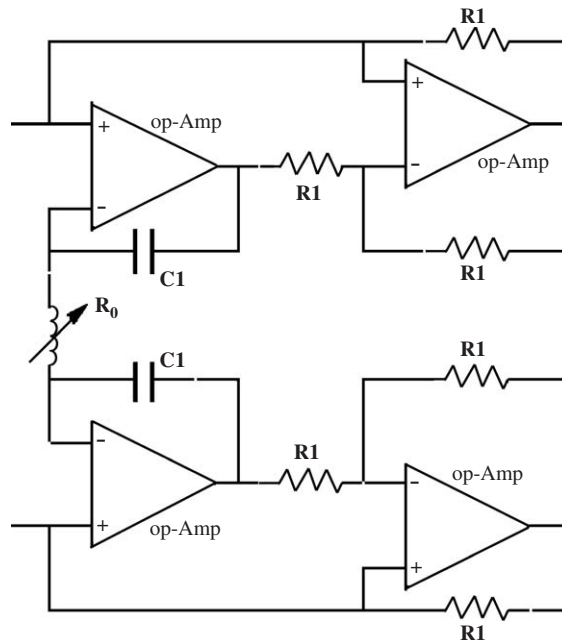
Fig. 9. Circuit diagram of the synthetic inductor.

The circuit diagrams of the synthetic inductor [30] and negative capacitor are shown in Figs. 9 and 10. From Fig. 9, the equivalent inductance value can be calculated as $L = R_1 R_0 C_1$ (Henry). In principle, any desired inductance value can be achieved by adjusting one component in the circuit, i.e., the potentiometer (R_0), with the other eight components fixed at appropriate values (R_1 and C_1). The negative capacitance circuit is essentially a negative-impedance converter (NIC) [31]. From Fig. 10, the equivalent negative capacitance value can be expressed as $C_n = -R_2 C_2 / R_2 = -C_2$. In order to increase the electromechanical coupling coefficient, each negative capacitance circuit will be connected in series with each piezoelectric patch. Since the negative capacitance circuit needs to be grounded, it is inserted between the negative electrode of each piezoelectric patch and the ground.

6.2. Experimental results

A sample frequency response function (FRF) of the mistuned bladed disk is shown in Fig. 11. The figure shows high modal density within the frequency range from 190 to 250 Hz, which is a characteristic feature of mistuned periodic structures. Due to this feature, it is very difficult to obtain mode shapes using common modal analysis methods. Therefore, alternatively, the amplitudes of blade tips when the bladed disk is under
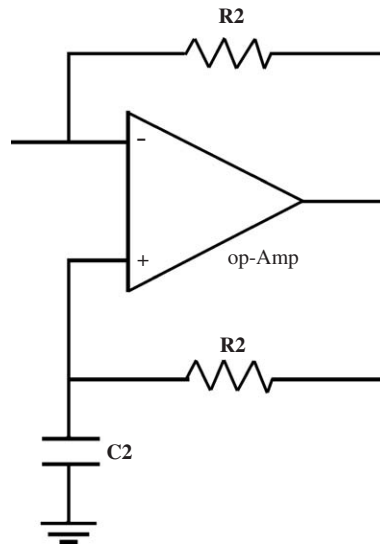
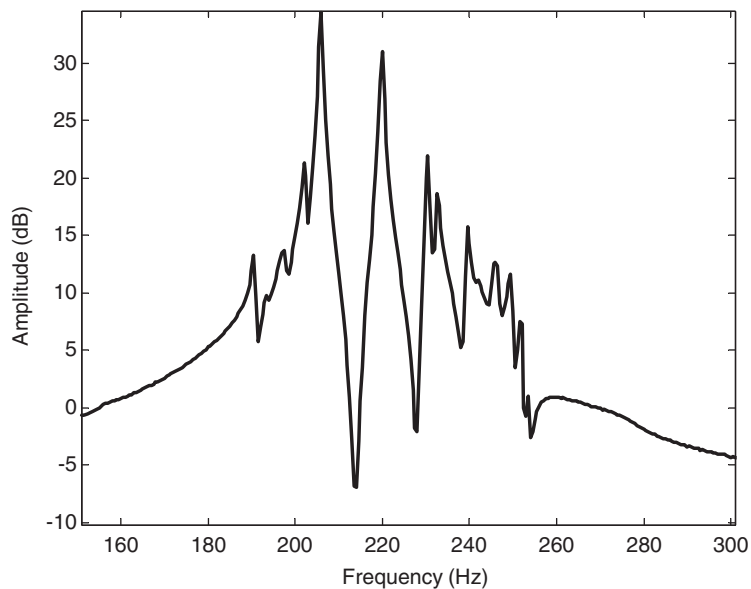Fig. 10. Circuit diagram of the negative capacitor.

Fig. 11. Sample frequency response of the mistuned bladed disk without circuit network.

harmonic excitation at resonant frequencies are chosen as comparison objectives in evaluating the delocalization effect of the piezoelectric circuit network. To excite the bladed disk at resonance, a series of frequencies within the range of 190–250 Hz, most of which are where FRF exhibits a resonant peak, are used for sine wave excitations.

In the preliminary test, it was found that under excitation frequency of 193.5 and 202.3 Hz, the amplitude distribution shows obvious localization phenomena, illustrated by the dotted lines in Figs. 12 and 14. In this investigation, we will thus focus our attention around these two resonant frequencies, and compare the amplitude distribution of the mistuned bladed disk with and without piezoelectric circuit network.
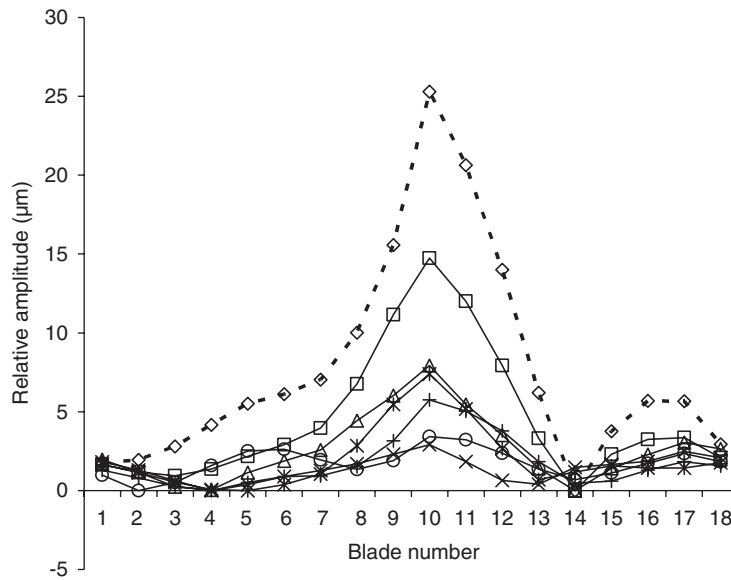
Fig. 12. Relative amplitudes of 18 blades for mistuned bladed disk without network and with network at various circuit frequency tunings (f_e) from 193.5 to 234 Hz. Legends: dotted line: ($\diamond$) without network; solid lines: ($\square$) $f_e = 193.5$ Hz; ($\triangle$) $f_e = 201$ Hz; ($\times$) $f_e = 206$ Hz; (*) $f_e = 212$ Hz; ($\circ$) $f_e = 222$ Hz; and (+) $f_e = 234$ Hz.

First, the mistuned bladed disk without circuit network is excited at 193.5 Hz. The tip displacements of all the 18 blades are measured with the laser vibrometer. Then the circuit network is connected to the piezoelectric patches on the bladed disk. The network has 18 synthetic inductors tuned to the same value. The circuit frequency, defined as $f_e = 1/\sqrt{LC_p}/2\pi$ (Hz), where C_p is the piezoelectric capacitance, can be tuned to different values by adjusting the synthetic inductance (L). Six different circuit frequency tunings are investigated, ranging from 193.5 to 234 Hz (corresponding to the non-dimensional parameter δ of range 0.88–1.06, which is covered in Fig. 7), as shown in Fig. 12. At each circuit frequency, the resonant response amplitudes of the blade tips are measured. These amplitudes are plotted in Fig. 12 for the mistuned bladed disk with and without circuit network. The amplitude data shown in this figure reflect the "*relative amplitude*" (the relative amplitude of each blade is defined to be the difference between its absolute amplitude and the lowest amplitude among all the 18 blades), which also applies to all other figures showing amplitude hereafter. It should be noted that when the piezoelectric circuit network is connected to the mistuned bladed disk, the resonant frequencies are slightly changed. In order to maintain the resonant excitation, for each particular circuit frequency tuning (f_e), the new resonance of the system is identified and the structure is excited at the new resonant frequency. This also applies to the case when negative capacitance circuits are introduced into the network.

The dotted data line in Fig. 12 shows that the relative vibration amplitudes are high over a small region (only 4–5 blades) around blade number 10. Outside this region, amplitudes are relatively small. This indicates that vibration is highly localized in the mistuned bladed disk. With the treatment, the solid lines corresponding to various circuit tunings show a more even distribution of the amplitudes over the 18 blades. This more even amplitude distribution indicates a reduction of the level of localization.

As a tool to quantify how the amplitude data is distributed spatially, standard deviations are plotted in Fig. 13. However, it should be noted that the standard deviation is not used as an exact index for quantifying localization, but only as a measurement of the scatterness of the amplitude data distribution. As Fig. 13 shows, the standard deviations for the mistuned bladed disk with treatment are much smaller than that without treatment.

Moreover, the delocalization effect of the piezoelectric circuit network is also demonstrated when the mistuned bladed disk is excited under the resonant frequency of (and around) 202.3 Hz. Resonant response amplitudes for the mistuned bladed disk with and without piezoelectric network are plotted in Fig. 14.
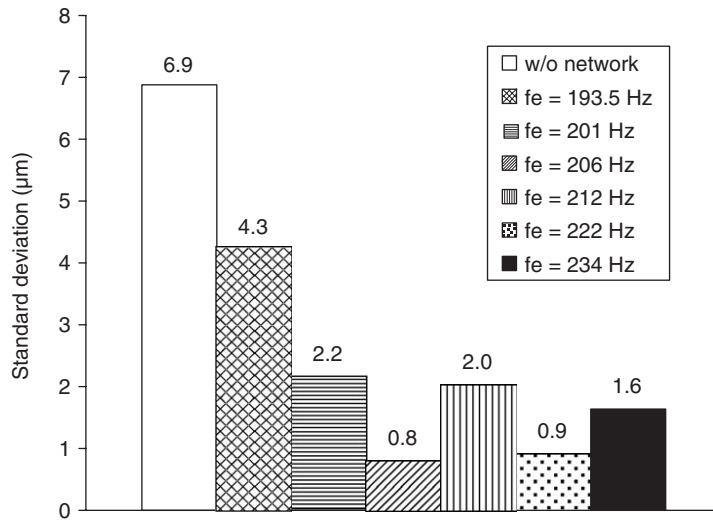
Fig. 13. Standard deviations of blade relative amplitudes for the system without network (first column) and with network at various circuit frequency tunings (f_e) (all other columns).
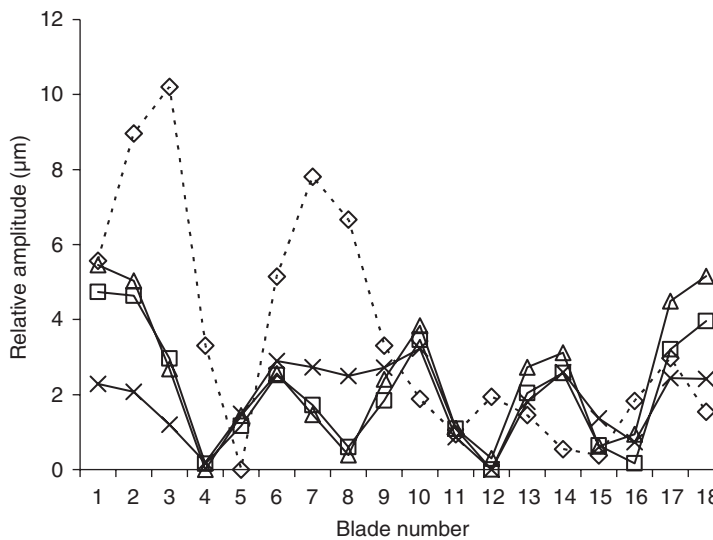

Fig. 14. Blade relative amplitudes distribution for the system without network (dotted line) and with network (solid lines) at resonances around 202.3 Hz. Legends: ($\diamond$) without network; ($\square$) $f_e = 201$ Hz; ($\triangle$) $f_e = 206$ Hz; and ($\times$) $f_e = 222$ Hz.

Without network, blade amplitudes are confined only in small regions around blade number 2, 3 and 7. With the piezoelectric circuit network (at three circuit frequency tunings: $f_e = 201$, 206, and 222 Hz), the blade amplitudes again become more evenly distributed over the 18 blades, which means the level of localization is reduced.

Next, negative capacitance circuits are incorporated into the piezoelectric network, and their effects on the delocalization performance are examined. The analytical results suggest that the electromechanical coupling coefficient (ξ) of the piezoelectric patch can be increased by the negative capacitance. As a result of this coupling enhancement, the overall delocalization effect of the piezoelectric circuit network can be further improved. To validate this prediction, negative capacitance circuits are built and connected in series with piezoelectric patches to the negative electrodes. The same experimental approach used in Ref. [26] is adopted

here to measure the electromechanical coupling coefficient. The value of ξ is calculated according to $\xi = \sqrt{((\omega^D)^2 - (\omega^E)^2)/(\omega^D)^2}$, which is based on the resonant frequencies of the substructure under open circuit condition (ω^D) and short circuit condition (ω^E) [28]. Note that this formula is exactly the definition of the electromechanical coupling coefficient at the structural level. The original electromechanical coupling coefficient of the piezoelectric patch is measured to be $\xi = 0.1224$. With a negative capacitance of $C_n = -4.7$ nF, the coupling coefficient is measured to be $\xi = 0.1930$, which is a 57.7% increase. This range of ξ is covered in the analytical study shown in Fig. 7.
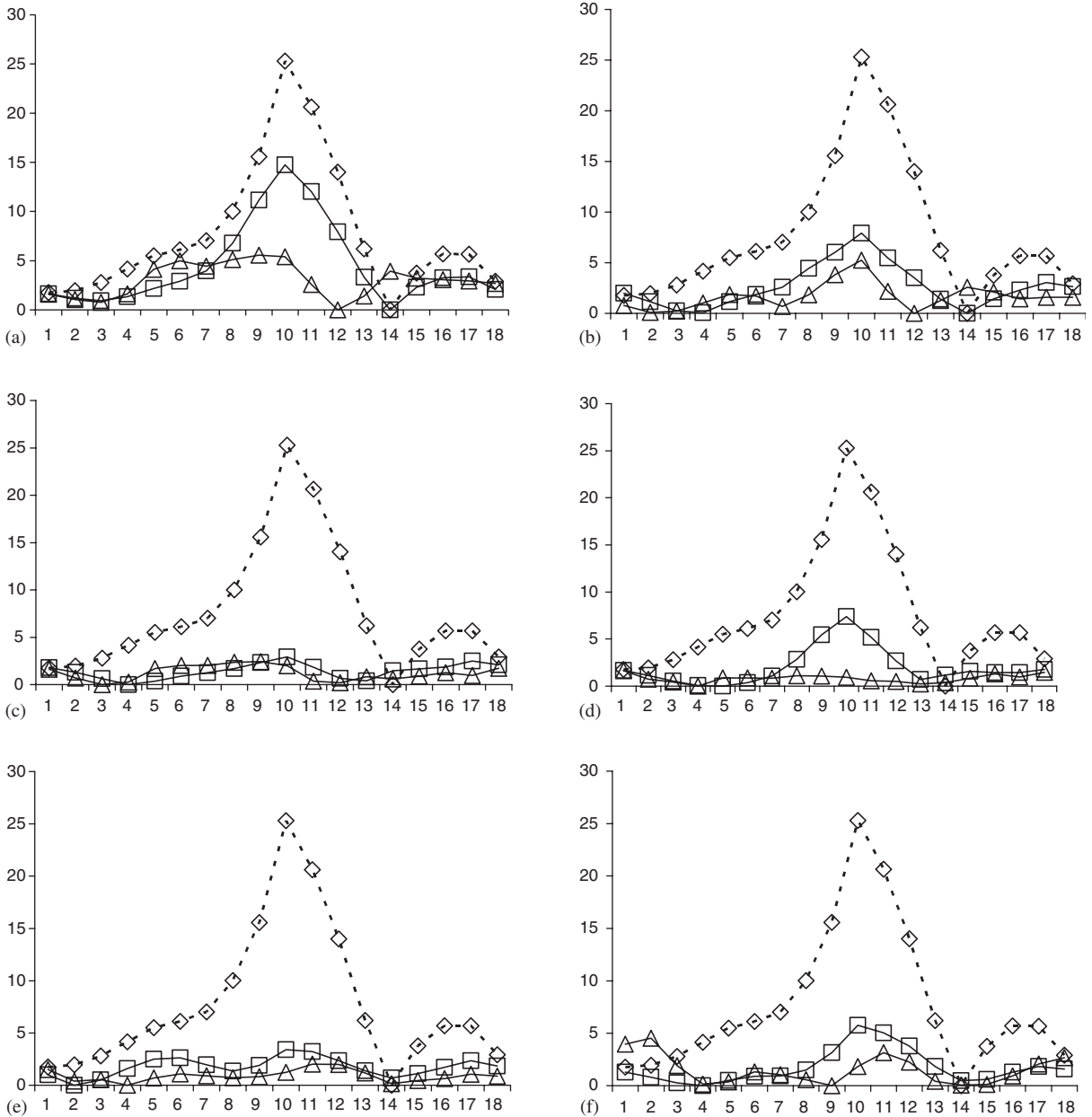

Fig. 15. Blade relative amplitudes of system without network ($\diamond$ in dotted line); with network ($\square$ in solid line); and with network augmented by negative capacitance ($\triangle$ in solid line); (a) $f_e = 193.5$ Hz; (b) $f_e = 201$ Hz; (c) $f_e = 206$ Hz; (d) $f_e = 212$ Hz; (e) $f_e = 222$ Hz; (f) $f_e = 234$ Hz; Horizontal axis: blade number; Vertical axis: relative amplitude (unit: μm).

Eighteen negative capacitance circuits with the same value ($C_n = -4.7\,\text{nF}$) are then built and integrated into the piezoelectric network. The network with negative capacitance is also referred to as the *augmented network*. Tip displacements of the 18 blades are re-measured for bladed disk with this augmented network. Resonant response amplitudes are compared to previous results shown in Figs. 12 and 14 in order to evaluate the delocalization performance improvement. First, the responses at the resonance around 193.5 Hz are examined and amplitudes are plotted in Figs. 15(a)–(f), with each corresponding to a circuit frequency tuning (f_e). It can be seen that for all of these six circuit frequency tunings, the vibration amplitude distributions with the augmented piezoelectric network become more uniform. This is predicted because with negative capacitance, the network has a larger electromechanical coupling (ξ). Therefore, the network is capable of transforming more mechanical energy into electrical form, which is then propagated throughout the network by the coupling capacitors. Again, the standard deviations of the amplitudes are calculated and shown in Fig. 16 for the mistuned bladed disk without any treatment, with network but no negative capacitance, and with the augmented network, marked as Case 1, Case 2 and Case 3, respectively. The decreasing trend of the standard deviations from Case 1 to Case 3 indicates that vibration amplitudes become more and more evenly distributed. These results show that the delocalization ability of the piezoelectric network is improved by the integrated negative capacitance circuits. Amplitudes of the mistuned bladed disk under resonant excitation frequencies of (and around) 202.3 Hz are also compared for Cases 1, 2 and 3, as shown in Figs. 17(a) and (b), with $f_e = 201$ and 206 Hz, respectively. Both figures show that amplitude localization is further reduced and
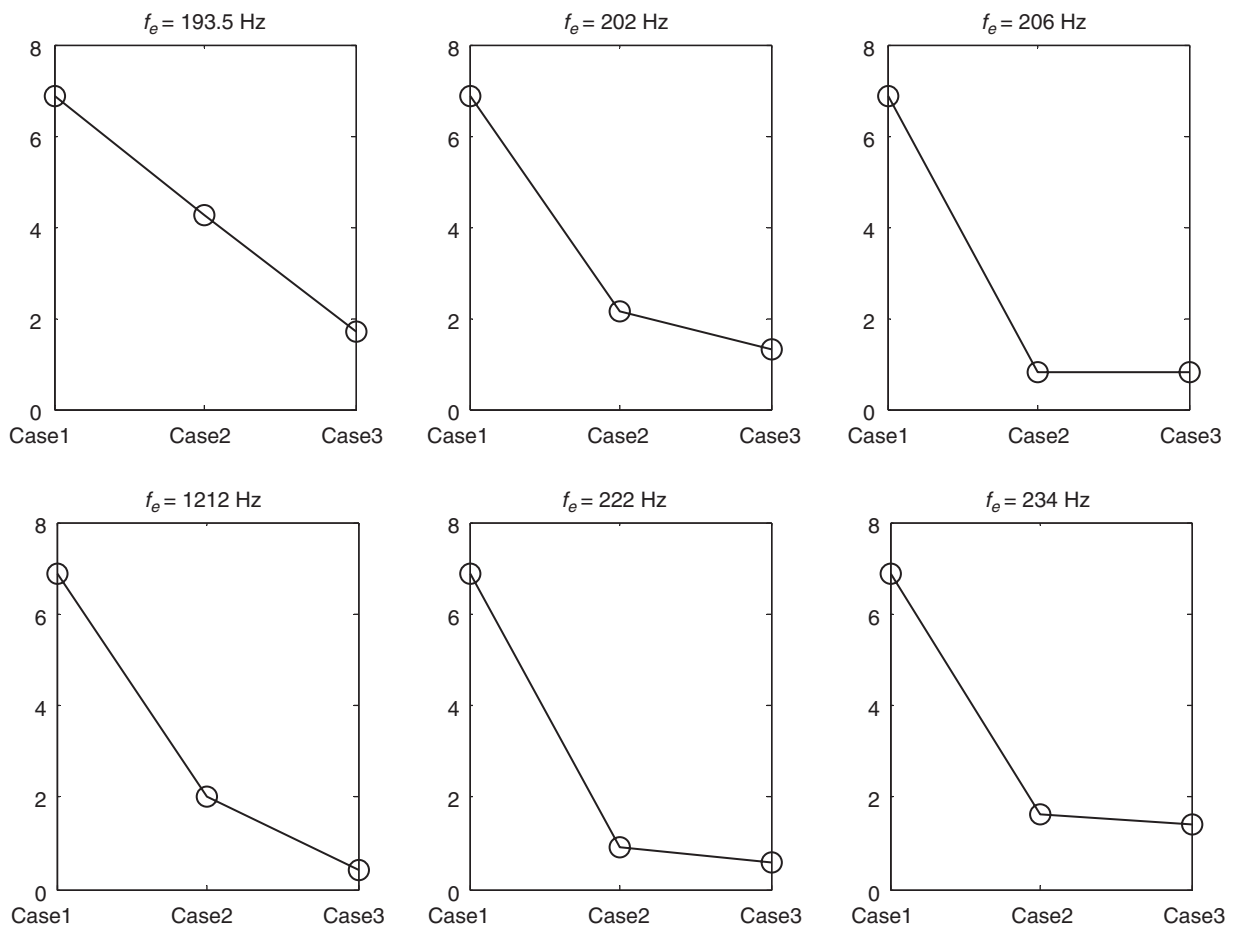

Fig. 16. Standard deviations of blade relative amplitudes for Case 1—mistuned bladed disk without network; Case 2—with network; and Case 3—with network augmented by negative capacitance circuits. Vertical axis: standard deviation (unit: μm).
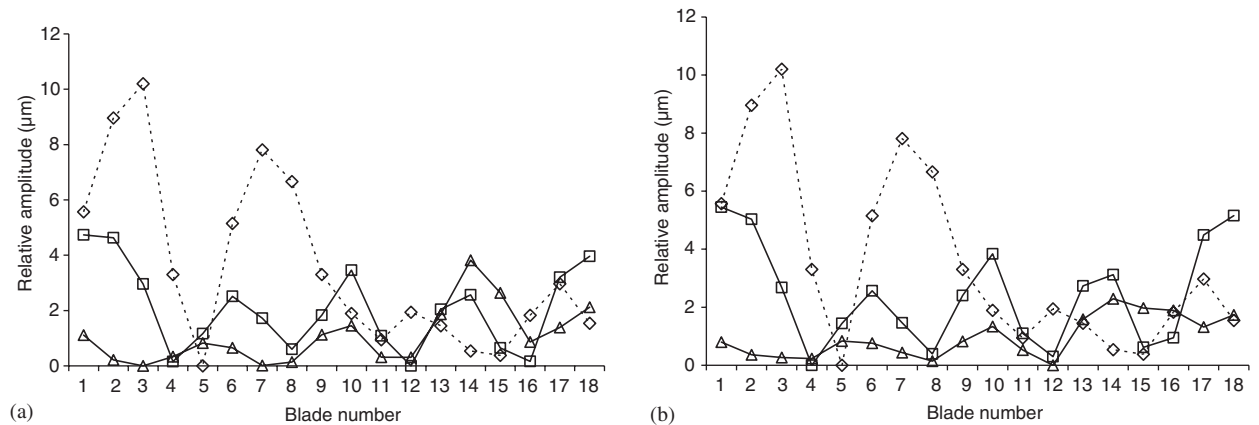
Fig. 17. Relative amplitudes distribution for the system without network ($\diamond$ in dotted line), with network ($\square$ in solid line) and with network augmented by negative capacitance ($\triangle$ in solid line): (a) $f_e = 201$ Hz; and (b) $f_e = 206$ Hz.

the distribution is more even for Case 3, as compared to that of Case 2. The results again illustrate improvements in the delocalization performance when negative capacitance circuits are added.

7. Conclusion

This paper presents vibration delocalization study of nearly periodic structures using piezoelectric networks with negative capacitance circuitry for active coupling enhancement. The correlation between the Lyapunov exponents and the spatial exponential decay of the modal amplitudes is studied. A localization index is defined for the bi-coupled nearly periodic system and applied to evaluate the effectiveness of the proposed scheme. With this localization index, a parametric study was performed where it was found that the negative capacitance circuit approach can greatly enhance the system's ability for vibration delocalization. It can effectively increase the electromechanical coupling coefficient, such that more localized mechanical energy can be transferred into electrical form and eventually distributed through the strongly coupled electrical circuits. This network is then implemented and integrated with a mistuned bladed disk and investigated experimentally to validate the analytical predictions. From the experimental results, it is shown that the level of localization can be reduced by using the piezoelectric network over a range of circuit frequency tunings. It is also illustrated that the apparent electromechanical coupling coefficient of the system can be increased by the negative capacitance, and the delocalization effect of the network can be further enhanced.

While this research has shown promising result for mode delocalization, it should be noted that under forced vibration circumstances, the dynamic phenomena could be more complicated, as seen in Ref. [20]. Thus the requirement for the piezoelectric network design under forced vibration could be different, which will be addressed in the future.

Acknowledgements

References

[1] C.H. Hodges, Confinement of vibration by structural irregularity, *Journal of Sound and Vibration* 82 (3) (1982) 411–424.

[2] S.S. Mester, H. Benaroya, Periodic and near-periodic structures, *Shock and Vibration* 2 (1) (1995) 69–95.

[3] C. Pierre, M.P. Castanier, W.J. Chen, Wave localization in multi-coupled periodic structures: application to truss beams, *Applied Mechanics Review* 49 (2) (1996) 65–86.

[4] J.C. Slater, G.R. Minkiewicz, A.J. Blair, Forced response of bladed disk assemblies—a survey, *The Shock and Vibration Digest* 31 (1) (1999) 17–24.

[5] C. Pierre, E.H. Dowell, Localization of vibrations by structural irregularity, *Journal of Sound and Vibration* 114 (1987) 549–564.

[6] S.-T. Wei, C. Pierre, Localization phenomena in mistuned assemblies with cyclic symmetry part I: free vibrations, *ASME Journal of Vibration, Acoustics, Stress and Reliability in Design* 110 (1988) 429–438.

[7] P.J. Cornwell, O.O. Bendiksen, Localization of vibrations in large space reflectors, *AIAA Journal* 27 (2) (1989) 219–226.

[8] C. Pierre, P.D. Cha, Strong mode localization in nearly periodic disordered structures, *AIAA Journal* 27 (2) (1989) 227–241.

[9] C.H. Hodges, J. Woodhouse, Vibration isolation from irregularity in a nearly periodic structure: theory and measurements, *Journal of Acoustical Society of America* 74 (3) (1983) 894–905.

[10] C.H. Hodges, J. Woodhouse, Confinement of vibration by one-dimensional disorder, I: theory of ensemble averaging, *Journal of Sound and Vibration* 130 (2) (1989) 253–268.

[11] C. Pierre, Weak and strong vibration localization in disordered structures, *Journal of Sound and Vibration* 126 (3) (1990) 485–502.

[12] P.D. Cha, C. Pierre, Vibration localization by disorder in assemblies of monocoupled, multimode component systems, *ASME Journal of Applied Mechanics* 58 (4) (1991) 1072–1081.

[13] D. Bouzit, C. Pierre, Vibration confinement phenomena in disordered, mono-coupled, multi-span beams, *ASME Journal of Vibration and Acoustics* 114 (4) (1992) 521–530.

[14] D.J. Mead, Wave propagation and natural modes in periodic systems: I. Mono-coupled systems, *Journal of Sound and Vibration* 40 (1) (1975) 1–18.

[15] D.J. Mead, Wave propagation and natural modes in periodic systems: II. Multi-coupled systems, with and without damping, *Journal of Sound and Vibration* 40 (1) (1975) 19–39.

[16] G.J. Kissel, Localization factor for multichannel disordered systems, *Physics Review A* 44 (2) (1991) 1008–1014.

[17] M.P. Castanier, C. Pierre, Lyapunov exponents and localization phenomena in multi-coupled nearly periodic systems, *Journal of Sound and Vibration* 183 (3) (1995) 493–515.

[18] W.-C. Xie, S.T. Ariaratnam, Vibration mode localization in disordered cyclic structures, I: single substructure mode, *Journal of Sound and Vibration* 189 (5) (1996) 625–645.

[19] W.-C. Xie, S.T. Ariaratnam, Vibration mode localization in disordered cyclic structures, II: multiple substructure mode, *Journal of Sound and Vibration* 189 (5) (1996) 647–660.

[20] M.P. Castanier, C. Pierre, Using intentional mistuning in the design of turbomachinery rotors, *AIAA Journal* 40 (10) (2002) 2077–2086.

[21] R.W. Gordon, J.J. Hollkamp, An experimental investigation of piezoelectric coupling in jet engine fan blades, in: *Proceedings of the Collection of Technical Papers—AIAA/ASME/ASCE/AHS/ASC Structures, Structural Dynamics and Materials Conference*, Vol. 1 (III), 2000, pp. 1975–1983.

[22] A.M. Cox, G.S. Agnes, A statistical analysis of space structure mode localization, in: *Proceedings of the 1999 AIAA/ASME/ASCE/AHS/ASC Structures, Structural Dynamics, and Materials Conference and Exhibit*, Vol. 4, 1999, pp. 3123–3133.

[23] G.S. Agnes, Piezoelectric coupling of bladed-disk assemblies, *Proceedings of the SPIE, Smart Structures and Materials* 3672 (1999) 94–103.

[24] J. Tang, K.W. Wang, Vibration delocalization of nearly periodic structures using coupled piezoelectric networks, *ASME Journal of Vibration and Acoustics* 125 (1) (2003) 95–108.

[25] J. Zhang, K.W. Wang, Electromechanical tailoring of piezoelectric networks for vibration delocalization and suppression of nearly periodic structures, in: *Proceedings of the 13th International Conference on Adaptive Structures and Technologies*, Potsdam, Berlin, Germany, 2002, pp. 199–212.

[26] J. Tang, K.W. Wang, Active–passive hybrid piezoelectric networks for vibration control: comparisons and improvement, *Journal of Smart Materials and Structures* 10 (4) (2001) 794–806.

[27] Institute of Electrical and Electronics Engineers, IEEE Standard on Piezoelectricity (ANSI/IEEE Std. 176-1987), IEEE, New York, 1988.

[28] G.A. Lesieutre, C.L. Davis, Can a coupling coefficient of a piezoelectric device be higher than those of its active material?, *Journal of Intelligent Material Systems and Structures* 8 (1997) 859–867.

[29] A. Wolf, J.B. Swift, H.L. Swinney, J.A. Vastano, Determining Lyapunov exponents from a time series, *Physica D* 16 (1985) 285–317.

[30] W. Chen, *Passive and Active Filters, Theory and Implementation*, Wiley, New York, 1986.

[31] P. Horowitz, W. Hill, *The Art of Electronics*, second ed., Cambridge University Press, Cambridge, 1989.